Ecological Indicators 131 (2021) 108180

Contents lists available at ScienceDirect

Ecological Indicators

journal homepage: www.elsevier.com/locate/ecolind

Remote sensing estimation of the concentration and sources of coloured dissolved organic matter based on MODIS: A case study of Erhai lake

Hao Zhang [a,b], Bo Yao [c], Shengrui Wang [a,b,*], Guoqiang Wang [b]

[a] Guangdong-Hong Kong Joint Laboratory for Water Security, Center of Water Research, Beijing Normal University, Zhuhai 519087, China
[b] Engineering Research Center of Ministry of Education on Groundwater Pollution Control and Remediation, College of Water Sciences, Beijing Normal University, Beijing 100875, China
[c] Key Laboratory for Mechanics in Fluid Solid Coupling Systems, Institute of Mechanics, Chinese Academy of Sciences, Beijing 100190, China

ARTICLE INFO

Keywords:
CDOM
Fluorescence index
Empirical algorithm
Semi-empirical algorithm
Erhai Lake

ABSTRACT

The use of satellite remote sensing to estimate coloured dissolved organic matter (CDOM) and identify its potential sources is important for monitoring lake water quality and implementing management strategies. In this study, taking Erhai Lake as an example and based on MODIS/Aqua satellite images and in-situ measured data, we used empirical and semi-empirical methods to develop algorithms for CDOM and the fluorescence index (FI_{370}) from remote sensing reflectance (Rrs(λ)). The temporal and spatial distributions of the CDOM concentration and FI_{370} in Erhai Lake during 2013–2019 were retrieved. The results show the following. (1) The band ratio (Rrs(469)+Rrs(645))/Rrs(555) model could estimate the CDOM absorption coefficient at 412 nm ($a_{CDOM}(412)$) (R^2=0.507), and it was relatively stable. Using the band ratio Rrs(645)/Rrs(469) combined with the chlorophyll-a (Chl-a) APProach by ELimination (APPEL) model, a semi-empirical inversion model of FI_{370} performed with satisfactory accuracy (R^2=0.550) and was more accurate than the empirical algorithm (R^2=0.505). (2) During the period of 2013–2019, the CDOM concentration in Erhai Lake generally decreased from the northern to the central to the southern parts of the lake, and the CDOM concentration was higher in summer and autumn than in spring and winter. FI_{370} was higher in the northern and western coastal waters and lower in the central, southern and eastern parts of the lake. FI_{370} in autumn and winter was higher than that in spring and summer. CDOM was affected by both terrestrial and internal sources, and their relative contributions were not the same in different seasons. (3) For different Chl-a concentrations, different CDOM concentration models had better retrieval effects, i.e., Rrs(645))/Rrs(555) and (Rrs(469)+Rrs(645))/Rrs(555) had the best performance when Chl-a<10 μg/L and Chl-a>10 μg/L, respectively. The inversion models established in this study offer improved quantifications of the CDOM concentration and the FI_{370} in Erhai Lake, providing important support for monitoring water quality and implementing efficient management strategies.

1. Introduction

Coloured dissolved organic matter (CDOM) is an important part of dissolved organic matter (DOM), and the CDOM composition and content can reflect the primary productivity of water bodies and have an important impact on the carbon balance of aquatic ecosystems (Downing et al., 2009). CDOM restricts the penetration of UV-B into the water column and therefore impacts water colour and the spectral distribution of underwater light (Conmy et al., 2004), which can cause a series of water photochemical reactions (Matsuoka et al., 2012). Additionally, CDOM has unique fluorescence properties, and the contents and properties of fluorescent substances can provide reliable tracers for revealing CDOM sources and biogeochemical behaviour in the water environment (Fellman et al., 2010). In recent decades, measuring CDOM characteristics has mainly been done using ultraviolet–visible (UV–Vis) absorption spectroscopy and excitation-emission matrix fluorescence coupled with parallel factor analysis (EEM-PARAFAC) (Fellman et al., 2010; Huguet et al., 2009; Kowalczuk et al., 2005), and the fluorescence intensity (FI_{370}) of EEM fluorescence spectra has mainly been measured from the ratio of fluorescence intensity, which has been used in the study of DOM dynamics. The fluorescence intensity can be used to identify the sources of CDOM in rivers and lakes (Zhang et al., 2010). Although the

* Corresponding author at: Engineering Research Center of Ministry of Education on Groundwater Pollution Control and Remediation, College of Water Sciences, Beijing Normal University, Beijing 100875, China.
E-mail address: wangsr@bnu.edu.cn (S. Wang).

https://doi.org/10.1016/j.ecolind.2021.108180
Received 4 April 2021; Received in revised form 1 August 2021; Accepted 1 September 2021
Available online 15 September 2021

in-situ measurement of CDOM concentration and composition in water bodies can provide accurate data, it is more expensive and time-consuming, especially in determining distributions over multiple times and large scales. Despite there are some Limitations in remote sensing inversion, such as the segregation of spectral signatures for Chl-a, suspended particulate matter and CDOM is still a challenge because of the influence of these parameter on each other (Gholizadeh et al., 2016). At the same time the atmospheric interference also restricts the optical signals coming from waterbodies (Brezonik et al., 2005). But it is more practical to use remote sensing monitoring methods to estimate the CDOM in lakes on large scales. Remote sensing techniques make it possible to have spatial and temporal view of CDOM in lakes and more effectively and efficiently monitor the waterbodies, and quantify its changes (Chen et al., 2017a; Griffin et al., 2018).

Based on the unique fluorescence properties of CDOM and its preferential absorption of UV–Vis light (Zhang et al., 2020), satellite remote sensing, which has broad spatial coverage and repeated observations, can be used to explore the temporal and spatial patterns of CDOM and its sources (Brezonik et al., 2015; Chen et al., 2019b). At present, there are two main types of CDOM algorithms that are commonly used in studies of water bodies: empirical/semi-empirical methods and analytical/semi-analytical methods. Empirical algorithms are widely used and have high accuracy, but the complex debugging process and algorithm structure mean that these algorithms cannot clearly explain the mechanisms of CDOM variability. Since semi-empirical algorithms use the spectral characteristics of water colour parameters as a priori knowledge (Wang and Yang, 2019), they have a clear theoretical basis (Zhu et al., 2014), but they are affected by the optical characteristics and geographical location of the lake. To date, the remote sensing inversion for optically active substance in coastal and inland complex (case II) waters is still based on empirical methods, mainly developed through statistical methods (Cherukuru et al., 2016; Dörnhöfer and Oppelt, 2016; Gholizadeh et al., 2016). However, the current estimation algorithms for CDOM optical characteristics and fluorescent intensity are uncertain and the extent to which a particular band ratio works for lakes is poorly known (Gholizadeh et al., 2016). In recent years, MODIS have been widely used for retrieval of CDOM in some aquatic systems. Compared with other remote sensing satellites, MODIS provides daily monitoring and has proper spectral wavelengths and Spatiotemporal resolution, which can meet the needs of monitoring lakes among large-scale and revealing long-term variation, particularly in cloudy areas.

Erhai Lake is the second-largest plateau lake in southwestern China, it is an important source of drinking water, irrigation, and tourism for Dali in Yunnan Province. It is characterized by its plateau geography, relatively deep water, and lower nutrient content (Ji et al., 2017; Liu et al., 2015a). But in recent decades, it is strongly affected by human activities (Lin et al., 2020), many agricultural pollutants enter the lake, resulting in an increase in organic matter in the water body (Zhang et al., 2018a). In addition, as phytoplankton grow, they take up nutrients and carbon and eventually decay, adding organic matter into the lake (Aurin and Dierssen, 2012), which enhances eutrophication in the receiving aquatic ecosystems. Therefore the ecological environment in the water is gradually deteriorating. At present, many studies have used ultraviolet absorption and fluorescence spectroscopy to analyse CDOM in lakes (Chen et al., 2011a; Kowalczuk et al., 2005; Lei et al., 2019; Chiu et al., 2019), but it is still a challenge to determine changes in CDOM concentrations and map the distribution of CDOM sources information over a large scale and a long period. Miao et al. used remote sensing technology to quantify the dynamic changes in the peak intensity of DOM fluorescence and developed a new algorithm to study the sources of CDOM in Lake Taihu, which provided a new idea for CDOM remote sensing research (Miao et al., 2019).

In this study, CDOM concentration and FI_{370} models were developed using MODIS/Aqua data to compare and analyse the estimation effects of these algorithms, which can estimate the CDOM concentration and sources information. Our approach strived to accurately quantify the concentration and sources of CDOM in Erhai Lake and further analysed the spatial and temporal distribution and influencing factors to provide theoretical and practical references for the protection and management of Erhai Lake.

2. Materials and methods

2.1. Study area

Erhai Lake is located in the Dali Bai Autonomous Prefecture of Yunnan Province (E99°32′–100°27′, N25°25′–26°16′). It is the seventh largest freshwater lake in China (Fig. 1), with an area of 256 km^2, an average depth of 10.5 m, a volume of 27×10^8 m^3 (Li et al., 2020; Zhang et al., 2018a). The main rivers entering the lake from the north are the Miju River, Luoshi River and Yong'an River. The Boluo River enters the lake from the south. From the west, eighteen streams flowing off Cangshan Mountain enter the lake, and the Xi'er River in the south is the only natural outflow of Erhai Lake (Wang et al., 2015a). The water depths in the northern and southern parts of the lake are relatively shallow, with distributed aquatic plants; the water depth in the centre is relatively deep, with basically no aquatic plant growth (Han et al., 2014). Agriculture is the main source of nonpoint source pollution, which is concentrated on the west bank of the lake, and all of these rivers have become polluted to varying degrees during recent economic development.

2.2. Field sampling and laboratory analysis

From 2013 to 2019, eight field cruises to Erhai Lake were completed in spring, summer, autumn and winter. A total of 45 sampling sites were set up from north to south according to the direction of water flow (see Fig. 1), and 94 samples were collected. Water samples were collected in 1L acid-washed plastic bottles at a depth of 0.5 m; the water samples were held on ice for processing in the laboratory. Each water sample (approximately 250–500 mL) was filtered with a prefired 0.7 μm GF/F filter (Whatman), collected in a brown glass bottle and stored at 4 °C for testing (Zhang et al., 2018b).

2.2.1. Absorption and fluorescence measurements of CDOM

The primary filtered water sample was filtered again using a 0.22-μm Millipore filter membrane to obtain the water sample for CDOM testing. A Shimadzu UV2600 spectrophotometer was used to measure the CDOM absorbance (Kowalczuk et al., 2005) using a 1-cm cuvette, relative to a reference of distilled water. Instrument scan settings were as follows: 250–750-nm wavelength scan range, fast scan speed; 1-nm sampling interval; and 0.5-nm slit width. The quartz cuvettes for blanks and samples were acid-soaked for one hour and then rinsed with distilled water and sample aliquots. Then, the absorption coefficient of each wavelength was calculated using Equation 1 as follows:

$$a_{CDOM}(\lambda) = 2.303D(\lambda)/l \quad (1)$$

where λ is the wavelength (nm), $a_{CDOM}(\lambda)$ is the absorption coefficient (m^{-1}), $D(\lambda)$ is the absorbance, and l is the optical path (m). In this study, the concentration of CDOM is expressed by the CDOM absorption coefficient at 412 nm (Alcântara et al., 2017; Mannino et al., 2014; Tehrani et al., 2013).

A Hitachi F-7000 fluorescence spectrometer with a 150-W xenon lamp and a voltage of 700 V as the excitation light source was used to perform three-dimensional fluorescence spectrum analysis on the filtered CDOM water samples. The excitation wavelength (Ex) was 200–550 nm, the slit width was 5 nm, and the increment was 5 nm; the emission wavelength (Em) was 280–550 nm, the slit width was 5 nm, the increment was 2 nm, and the scanning speed was 2400 nm/min. The blank spectrum was subtracted from the three-dimensional fluorescence spectra of all water samples to remove the effect of Raman scattering

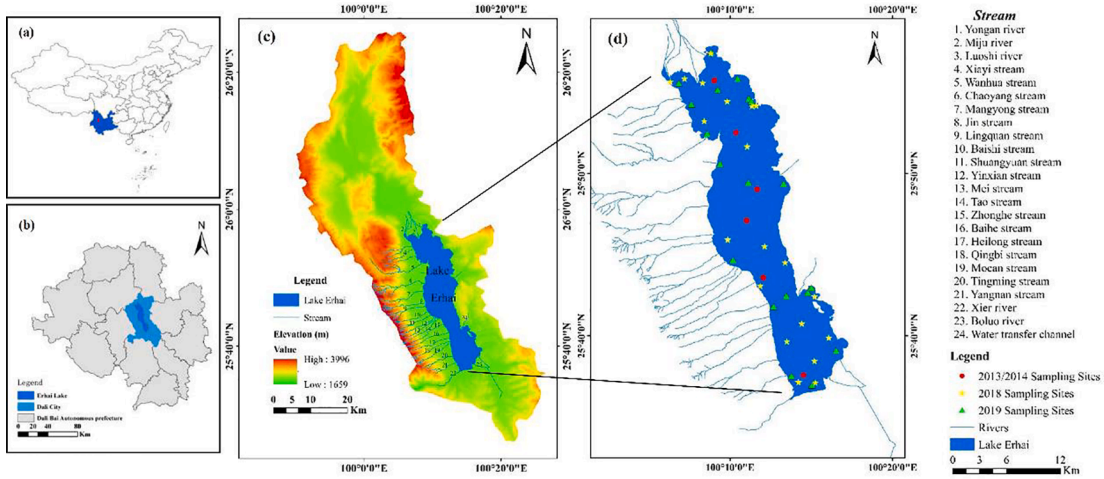

Fig. 1. (a) Location of Erhai Lake in China; (b) location of Erhai Lake in Dali Bai Autonomous Prefecture; (c) elevation map of Erhai Lake Basin; and (d) distribution of sampling points in Erhai Lake.

(Claustre et al., 2000; McKnight et al., 2001). In the spectral region where the emission wavelength was equal to the excitation wavelength or twice the excitation wavelength, the Rayleigh scattering and the spectral data above were assigned a value of 0 to eliminate the influence of Rayleigh scattering (Zepp et al., 2004).

2.2.2. Calculation of the fluorescence indices

To better understand the composition and sources of CDOM, different fluorescence indices were calculated. FI_{370} is the ratio of the fluorescence intensity at 450 and 500 nm in the fluorescence emission spectrum when the excitation light wavelength is 370 nm. FI_{370} can be used to distinguish the terrestrial and microbial sources of CDOM (McKnight et al., 2001) and is a simple and sensitive indicator of the sources of CDOM in water bodies. McKnight et al. suggested that $FI_{370}>1.9$ indicates that the CDOM is mainly derived from microbial metabolites in sediments, and $FI_{370}<1.4$ indicates that the CDOM is mainly derived from external input and the sedimentation of nutrients in the lake (McKnight et al., 2001). The humification index (HIX) is the ratio of the peak area of the emission wavelength of 435–480 nm to the fluorescence peak area of 300–345 nm when the excitation wavelength is 254 nm, which is used to characterise the degree of humification of organic matter. A higher HIX value means a higher degree of humification (Zsolnay et al., 1999). The biological index (BIX) is defined as the ratio of the fluorescence intensity emitted at 380 nm and 430 nm at an excitation wavelength of 310 nm. As the value increases, the CDOM has stronger endogenous characteristics, which is an indicator that reflects the proportion of self-generated contributions in the DOM (Huguet et al., 2009).

2.2.3. Measurement of other water quality parameters

The other measured water quality indicators were chlorophyll-a (Chl-a) and dissolved organic carbon (DOC). Chl-a was extracted with ethanol (90%) at 80 °C for 6 h in darkness and then analysed using a spectrophotometer (Shimadzu UV-3600) (Gitelson et al., 2008; O'Reilly and Werdell, 2019). The DOC concentration was measured by High Temperature Catalytic Oxidation (HTCO) on a Shimadzu TOC-5000A Analyzer, following the methods described in the literature (Downing et al., 2009; D'Sa et al., 2016).

2.3. In-situ measured data and satellite data

The statistics of the measured water quality data of Erhai Lake from 2013 to 2019 are shown in Table 1. The range of $a_{CDOM}(412)$ is 0.09–13.82 m^{-1}, the FI_{370} index ranges from 1.55 to 1.80, Chl-a ranges from 0.48 to 26.37 μg/L, and the DOC concentration ranges from 2.42 to 39.76 mg/L.

In this study, the MODIS/Aqua Level-1A data were downloaded from NASA's archive (https://oceandata.sci.gsfc.nasa.gov/) (Table S1). First, the cloud-free image of Erhai Lake was selected according to the sampling date (see Table 1). The downloaded MODIS Level-1A data were reprocessed using the SeaDAS software (version 7.3) to produce Level-1B and geo-location files (Hou et al., 2017; Klein et al., 2017; Wu et al., 2013). The Management Unit Mathematical Model (MUMM) was used to perform atmospheric correction, which is an extension of Gordon's standard atmospheric correction algorithm. The MUMM is useful for case 2 water (Ruddick et al., 2004). Then, images were processed using the ENVI 5.3 software, and the average value of the 3×3 pixels near the pixel where the sampling point coordinates were located was used for analyses.

2.4. Model development and accuracy assessment

Based on the in-situ data set, 3/4 of the total number of samples was randomly selected for modelling, and the remaining samples were used

Table 1
Water properties and dates of in-situ sampling and image acquisition.

Sampling Date	N	$a_{CDOM}(412)$ (m^{-1})	FI_{370}	Chl-a (μg/L)	DOC (mg/L)	Image Date
25/04/2013	6	—	1.69–1.80 (1.75 ± 0.04)	0.48–7.74 (3.56 ± 2.93)	3.27–4.27 (3.67 ± 0.35)	27/04/2013
10/07/2013	6	3.87–5.49 (4.15 ± 0.62)	1.64–1.75 (1.70 ± 0.03)	7.11–20.42 (13.07 ± 4.07)	4.32–6.98 (5.61 ± 0.97)	3/07/2013
18/10/2013	6	2.62–4.67 (3.76 ± 0.62)	1.63–1.69 (1.66 ± 0.02)	11.08–26.37 (16.05 ± 4.94)	2.42–4.77 (3.39 ± 0.78)	9/10/2013
03/01/2014	6	1.91–4.56 (3.77 ± 0.88)	1.66–1.69 (1.67 ± 0.015)	5.48–10.74 (7.72 ± 1.70)	6.26–7.93 (7.18 ± 0.60)	04/01/2014
05/09/2018	16	4.96–6.12 (5.45 ± 0.41)	1.55–1.65 (1.60 ± 0.04)	5.79–11.95 (8.85 ± 1.95)	5.02–5.99 (5.51 ± 0.26)	05/09/2018
11/04/2019	18	0.16–0.55 (0.37 ± 0.10)	1.54–1.67 (1.58 ± 0.04)	5.31–18.75 (8.80 ± 3.46)	5.67–39.76 (15.15 ± 11.23)	13/04/2019
06/05/2019	18	0.09–4.90 (0.89 ± 1.22)	1.39–1.68 (1.56 ± 0.06)	2.20–14.55 (11.12 ± 3.05)	4.43–30.65 (15.76 ± 8.10)	07/05/2019
04/06/2019	18	0.51–13.82 (2.40 ± 3.56)	1.63–1.70 (1.67 ± 0.03)	4.82–16.42 (11.48 ± 3.20)	6.74–37.61 (18.02 ± 9.13)	02/06/2019

to verify and evaluate the performance of the algorithms. The specific steps are as follows:

(1) According to previous studies, the bands that have high correlations with water quality parameters were determined by the characteristic spectrum.

(2) A series of band combinations were established using the MODIS band reflectance (Rrs), including addition, subtraction, multiplication, division and normalisation processing.

(3) A correlation analysis was performed for the field-measured data and the constructed band combinations using linear, exponential, logarithmic, and power functions for fitting; the optimal algorithm was determined according to the correlation coefficients. The inversion models of CDOM concentration and FI_{370} were developed as follows:

$$CDOM = b0 + \sum(bi \times band\ or\ combination) \quad (2)$$

$$FI_{370} = b0 + \sum(bi \times band\ or\ combination) \quad (3)$$

where b0 and bi are the coefficients of the fitting equation determined through regression analysis. Based on band combinations, the Chl-a concentration can also be introduced as a variable in the FI_{370} model because phytoplankton degradation has strong fluorescence properties (Wang et al., 2018; Zhang et al., 2009). Existing Chl-a remote sensing products use the APProach by ELimination (APPEL) model, which was proposed by EI-Alem et al. for the MODIS data source (El-Alem et al., 2012). Semi-empirical models eliminate the influence of blue and red light on the removal of CDOM and suspended matter by combining the characteristics of near-infrared band reflectivity, thus removing the effect of backscattering. The application of this model is relatively mature, and it has been verified in different areas, such as Lake Taihu and Lake Poyang. Additionally, the inversion performance for Chl-a in some lakes was better than in other models (Wang, 2015b; Xu et al., 2020a).

$$F(APPEL) = R(a_{NIR}) - [(R(a_{BLUE}) - R(a_{NIR})) * R(a_{NIR}) + R(a_{RED}) - R(a_{NIR})] \quad (4)$$

where F(APPEL) is the spectral index of APPEL and $R(a_{NIR})$, $R(a_{BLUE})$, and $R(a_{RED})$ are the near-infrared, blue, and red bands of the MODIS remote sensing data, respectively.

To evaluate the performance of the CDOM algorithm, the coefficient of determination (R^2), the adjusted coefficient of determination (Adj. R^2), the p-value, the root mean square error (RMSE) and the average absolute percentage difference (APD) were introduced as statistical indicators to validate the applicability and accuracy of the model. The definitions of RMSE and APD are given by the following equations, where i represents the current sample number, x_i represents the data estimated from the MODIS/Aqua data, y_i represents the data measured in the field, and n is the number of samples selected:

$$RMSE = \sqrt{\frac{1}{n-1}\sum_{i=1}^{n}(X_i - Y_i)^2} \quad (5)$$

$$APD = \frac{100}{n}\sum_{i=1}^{n}\left|\frac{X_i - Y_i}{Y_i}\right| \quad (6)$$

3. Results

3.1. Establishment and verification of the CDOM model

3.1.1. Development of the CDOM concentration algorithm

According to the optical characteristics of CDOM and the band settings of MODIS/Aqua, we selected the reflectance at 412 nm, 469 nm, 488 nm, 531 nm, 555 nm, 645 nm, 667 nm and 859 nm based on the method described in 2.4. The correlations between $a_{CDOM}(412)$ and the band combinations are shown in Table 2. The logarithmic model showed the best performance. Figure S1 shows the fitted relationships between $\ln(a_{CDOM}(412))$ and the band combinations. The data show that $\ln(a_{CDOM}(412))$ and (B3+B1)/B4 had good fitting results (R^2=0.57, RMSE=0.27 m^{-1}; Figure S1f); B4/B3 and $\ln(a_{CDOM}(412))$ also had a significant correlation (R^2=0.34), with a RMSE of 0.38 m^{-1}, which was higher than that of the (B3+B1)/B4 model. Therefore, this study chose (B3+B1)/B4 as the best band combination for estimating $a_{CDOM}(412)$, and $a_{CDOM}(412)$ was then calculated according to Equation (5).

$$Model\ 1:\ ln(a_{CDOM}(412)) = 6.577 - 3.71[(Rrs(645) + Rrs(469)/Rrs(555))] \quad (7)$$

3.1.2. Development of the FI_{370} algorithm

The FI_{370} model was developed according to the method described in 2.4, and the model was established by band combination. The results in Table 3 show that (B3-B4)/(B3+B4) performed the best. The results are shown in Fig. 2(a). In addition, the APPEL model was introduced on the basis of B1/B3 to establish a semi-empirical model (R^2=0.550, RMSE=0.037, APD=19.323%) (see the Fig. 2(b)). Model 3 had a better accuracy than Model 2, and FI_{370} was derived from Equations (8) and (9).

$$Model\ 2:\ FI_{370} = 1.571 - 0.205 \times (Rrs(469) - Rrs(555))/(Rrs(469) + Rrs(555)) \quad (8)$$

$$Model\ 3:\ FI_{370} = 1.505 + 0.094 \times [Rrs(645)/Rrs(469)] - 0.098 \times F(APPEL) \quad (9)$$

3.1.3. Model validation

Based on the remaining 1/4 of the verification data in the datasets, which were used to verify the robustness of the CDOM concentration

Table 2
Performances of the $a_{CDOM}(412)$ estimation models and results of the models analysis with different band combinations.

Algorithm	Band Ratio	Linear			Exponential			Logarithmic		
		R^2	RMSE	p	R^2	RMSE	p	R^2	RMSE	p
Green-blue Two-band ratio	B4/B3	0.14	0.90	0.001	0.35	0.87	0.000	0.34	0.38	0.000
	B10/B4	0.00	2.04	0.904	0.00	1.08	0.972	0.00	0.47	0.792
Green-red Two-band ratio	B1/B4	0.02	1.08	0.293	0.04	0.91	0.164	0.04	0.40	0.164
	B13/B4	0.09	1.04	0.036	0.07	0.90	0.082	0.07	0.39	0.082
NIR-red Two-band ratio	B2/B1	0.01	1.09	0.612	0.01	0.93	0.524	0.09	0.40	0.524
Green-blue Three band ratio	(B3+B1)/B4*	0.40	0.85	0.000	0.57	0.27	0.000	0.57	0.62	0.000
	(B3+B4)/B2	0.02	1.08	0.000	0.01	0.93	0.581	0.01	0.40	0.581
	(1/B3 +1/B4)/B2	0.00	1.09	0.759	0.00	0.93	0.684	0.06	0.40	0.684
	(1/B2+ 1/B3)/B4	0.00	1.09	0.686	0.03	0.92	0.266	0.03	0.40	0.266

*: This model was selected to estimate the $a_{CDOM}(412)$ in Erhai Lake in this study.

Table 3
FI_{370} models developed using different bands and band ratios.

Independent Variables	R^2	Equation Coefficients Y = b0 + b1(x1) + b2(x2) b0	b1	b2	Outlier	RMSE	Adj.R^2
FI_{370} models							
B13/B10	0.35	1.53	0.08			0.05	0.34
B3/B4	0.39	1.71	−0.14			0.05	0.38
B3/B1	0.21	1.67	−0.08			0.06	0.19
B3/B1,B11/B4	0.32	1.65	−0.08	0.04		0.06	0.29
(B3-B4)/(B3+B4)*	0.50	1.57	−0.21			0.03	0.48
B1/B3, F(APPEL)*	0.55	1.505	0.094	−0.098		0.04	0.53

*: This model was selected to estimate the FI_{370} in Erhai Lake in this study.

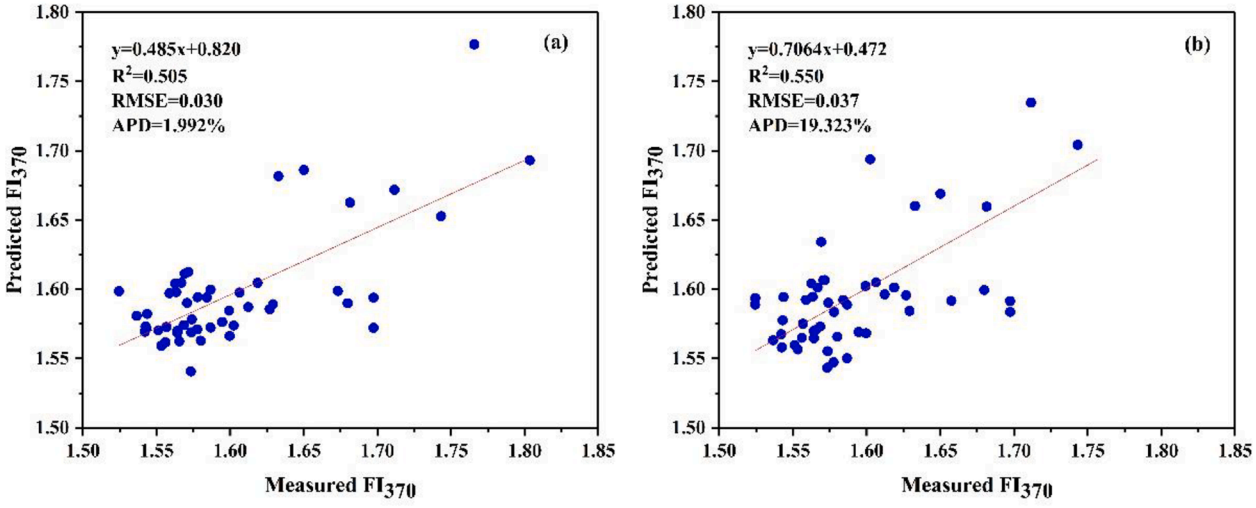

Fig. 2. Comparison between the predicted and measured values of FI_{370}: (a) empirical model; (b) semiempirical model.

and FI_{370} models, and the algorithm was evaluated by the RMSE and APD. The results are shown in Fig. 3. In the validation data set of $a_{CDOM}(412)$, the Model 1 results had higher accuracy (R^2=0.655, RMSE=0.435 m^{-1}, APD=47.717%). In the verification of the FI_{370} models, Model 3 (R^2=0.761, RMSE=0.025, APD=2.032%) had better prediction accuracy and lower error than Model 2 (R^2=0.479, RMSE=0.036, APD=2.989%). What's more, the measured $a_{CDOM}(412)$ and FI_{370} are significantly linearly correlated with the predicted values of the corresponding models and are uniformly distributed on both sides of the 1:1 line. The estimation accuracy indicated that the models had satisfactory performance and good applicability for the CDOM concentration and the FI_{370} of Erhai Lake. Therefore, it has been verified that the above models can be used to estimate the CDOM concentration and FI_{370} in Erhai Lake.

3.2. Temporal and spatial distributions of the CDOM concentration

The CDOM spatial distribution was generated by averaging all the

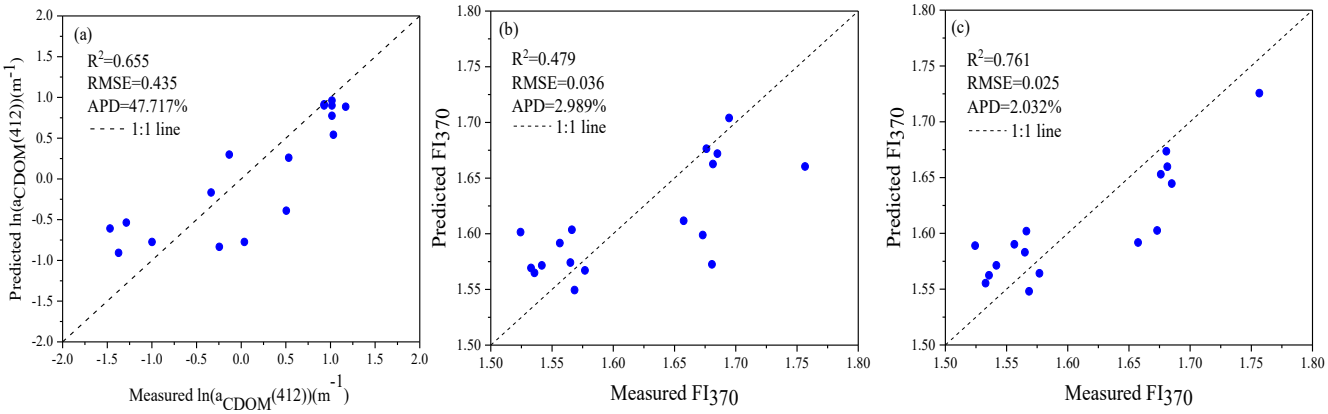

Fig. 3. Validation of the models and a comparison between the predicted and measured concentrations of the empirical and semi-empirical models of CDOM concentration and FI_{370}; (a) the validation of the estimated $a_{CDOM}(412)$ with the in situ measured $a_{CDOM}(412)$ based on Model 1; (b) the validation of the estimated FI_{370} with the in situ measured FI_{370} based on Model 2; (c) the validation of the estimated FI_{370} with the in situ measured FI_{370} based on Model 3.

MODIS/Aqua-derived CDOM concentration data for each of the 12 months in 2019 (Fig. 4). Overall, the $a_{CDOM}(412)$ exhibited spatial variations in Erhai Lake. The concentration of CDOM in the northern part of the lake was higher than that in the central and southern parts. Some areas with higher CDOM concentrations were distributed in the northern and western areas, where rivers enter the lake (the maximum was approximately 2.5 m^{-1}), and the southern part had lower CDOM (the minimum was approximately 0.3 m^{-1}). The water quality of the western littoral regions changed drastically over the year, and there were obvious differences in the spatial distribution of the CDOM concentrations in this area in different months. According to the previous research, the surface runoff carries a large number of terrestrial pollutants, especially organic matters, into the lake, which accepts 18-river inputs of the western surrounding areas (Yang et al., 2021). And it provides a material basis for the growth and reproduction of Aquatic phytoplankton, which can release extracellular DOM (Baines and Pace, 1991; Wang et al., 2020).

According to its morphological features, Erhai Lake was separated into five subregions: the northern, central-northern, central, central-southern, and southern regions; then, the CDOM concentration distribution of the entire lake and various regions in different seasons between 2013 and 2019 was performed derived from MODIS-Aqua data, which can help us obtain more accurate information about the dynamics and distribution of CDOM. In general, in time series, the $a_{CDOM}(412)$ in the entire lake ranged from 0.64 to 0.90 m^{-1}, with an average value of 0.81 ± 0.08 m^{-1}, and exhibited a small range fluctuating trend from 0.77 m^{-1} in 2013 to 0.85 m^{-1} in 2019 (Figure S2), but there were marked seasonal changes of $a_{CDOM}(412)$ in multiple years, which was relatively different over the four seasons, $a_{CDOM}(412)$ were the higher in summer and autumn, followed by spring, and the lowest in winter. A clear seasonal repetition was revealed by time series of seasonal mean $a_{CDOM}(412)$ for the whole of Erhai Lake (Fig. 5 and Figure S3). In spring,

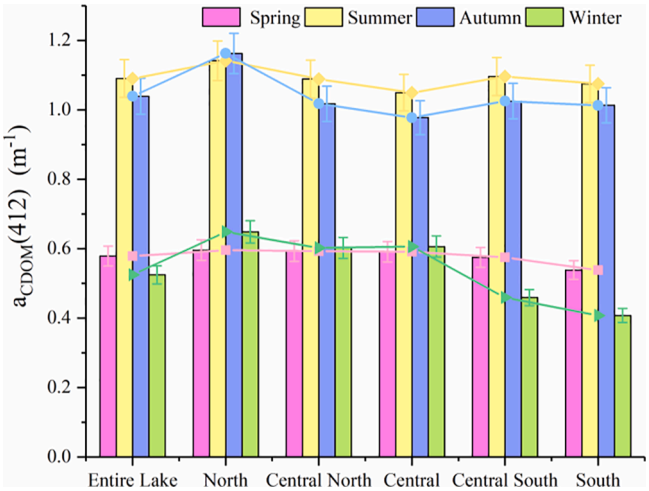

Fig. 5. Seasonal mean values of $a_{CDOM}(412)$ derived from MODIS/Aqua data for five lake regions and the entire lake from 2013 to 2019.

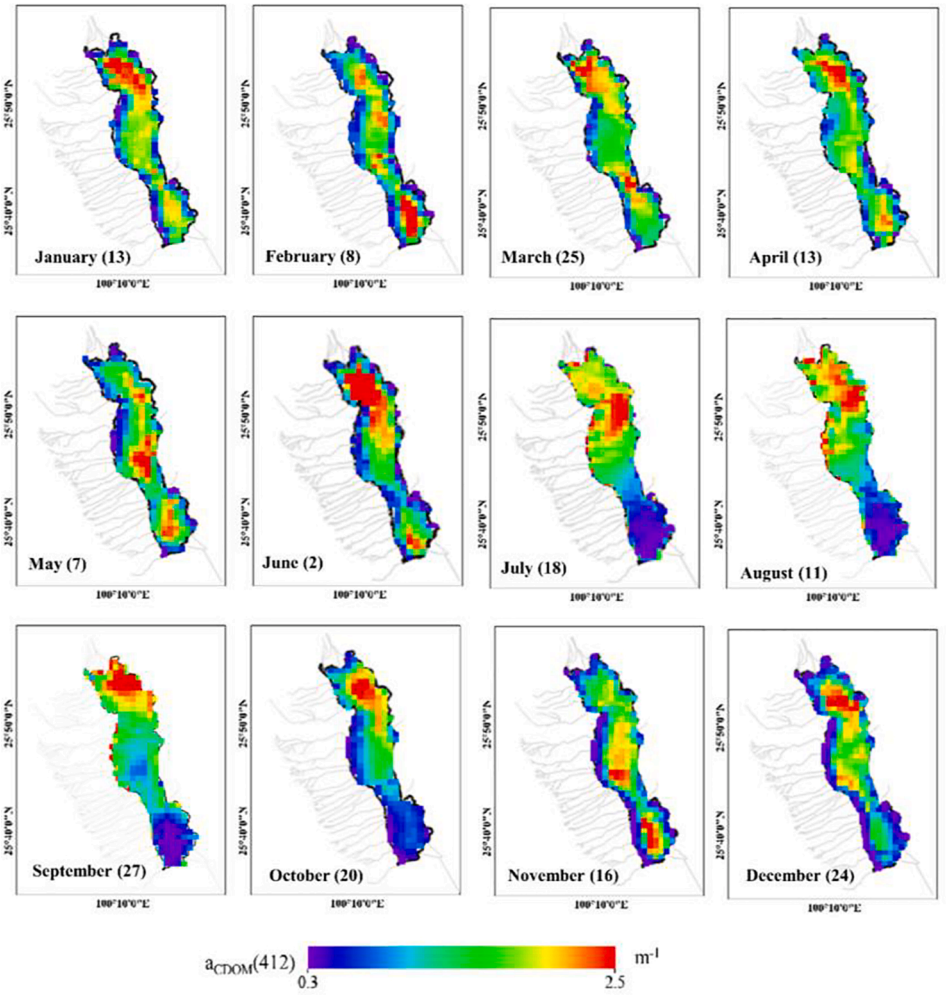

Fig. 4. Monthly distribution of $a_{CDOM}(412)$ in 2019 derived from the MODIS data.

the concentration of CDOM had little spatial variability in the entire lake which was about 0.6 m^{-1}. In summer and autumn, the CDOM concentration in the northern area of Erhai Lake was slightly higher than that in the central and southern areas. In winter, the concentration of CDOM in Erhai Lake was significantly different than in other seasons, showing a decreasing trend from north to south the south area had the lowest concentration of CDOM. In terms of spatial distribution, the five lake segments showed the same inter-annual variation pattern as the entire lake. The maximum value of the entire lake always appeared in the northern lake segment, ranging from 0.67 $m^{-1}$to 0.97 m^{-1}. The $a_{CDOM}(412)$ values of the northern and central-northern regions were clearly higher than those of the entire lake and other lake regions, which were approximately 2 times that in the southern part, probably because the only outflow of Erhai Lake is located in the south. Through lake self-purification by dilution (Guo et al., 2001), the concentration of CDOM decreased continuously. The concentration of CDOM during winter was lowest in the southern subregion.

In order to better analyze the change characteristics within the year, take 2019 as an example, this study focused on the monthly mean CDOM concentration in 2019. It exhibited distinct intermonth and spatial variations in 2019 (Fig. 6) and a high CDOM concentration in January. Because the water temperature was low and the lake water level was high in winter, a large amount of dead biological residue degraded to produce organic matter. From March to April, $a_{CDOM}(412)$ showed an obvious downward trend, which may be due to the gradual increase in water temperature and algal consumption of CDOM, resulting in a decrease in organic matter content in the lake water (Jing et al., 2019). Precipitation increased from May to July, and rivers entered the lake with exogenous organic matter. On the other hand, relatively high water level caused aquatic plants in the inundation area of the lakeside zone to decompose, which is another reason for the increase in CDOM in the lake (Fig. 6). Because CDOM is a type of material that photochemically degrades, a series of photochemical reactions occurs under ultraviolet irradiation. CDOM is degraded under strong sunlight in summer and absorbed by aquatic plants(Wen et al., 2016; Xue et al., 2019), which makes the concentration of CDOM decrease significantly in August. In autumn, the concentration of CDOM in the lake fluctuates greatly because Erhai Lake is affected by wind and waves, and resuspension causes the sediment to mix within the water column (Liu et al., 2013; Zhang and Zhi, 2020). Since aquatic plants continue to grow but also decay, the consumption of CDOM is reduced, and the ultraviolet radiation in autumn is significantly reduced, such that the CDOM concentration reaches its highest level throughout the year. From October to December, the concentration of CDOM shows a significant downward trend due to the massive death of phytoplankton and aquatic organisms in winter; the contribution of terrestrial sources to the lake was also significantly reduced.

3.3. Temporal and spatial distributions of FI_{370}

Monthly averaged FI_{370} values were produced for 2019. Fig. 7 shows that there are also differences in the temporal and spatial distributions of FI_{370}. In terms of time, FI_{370} was generally higher in autumn and winter than in spring and summer, which is consistent with the seasonal variations in CDOM concentration. There were notable differences from the northern to the southern lake regions, but the overall characteristics indicated terrestrial and biological sources. Lower values are mainly due to the release of sediment, while some areas with higher FI_{370} appear in the northern waters, which may be due to the main water source entering the lake from the north, as the river input causes algae to grow in large numbers in the northern bay of the lake (Lin et al., 2020). Due to the increase in temperature, the growth of algae and the increase in biological activity during spring and summer, the biomass of algae was high in October, with an evident biological source. Overall, the FI_{370} inversion results indicate that CDOM was mainly of biological origin, which verifies that biological sources are the main sources of CDOM in Erhai Lake.

According to the measured data in 2013, the changes in the fluorescence indices in different seasons are shown in Fig. 8. Comparing the changes of the fluorescence indices in different seasons, the order of FI is spring>summer>winter>autumn, the order of BIX is summer>autumn>winter>spring, and the order of HIX is autumn>winter>spring>summer, which indicates that the source and composition of CDOM vary greatly in different seasons. Overall, FI_{370}, which fluctuated between 1.66 and 1.72, demonstrated distinct variations and showed an overall decreasing trend from north to south, indicating that the CDOM of Erhai Lake was transformed from a terrestrial origin to a biological origin. The BIX of Erhai Lake showed an overall increasing trend from north to south, fluctuating between 1.01 and 1.21, indicating that biological activity led to an increase in the proportion of self-generating sources from north to south in Erhai Lake; the result for BIX is the same as that for FI. HIX showed a relatively weak degree of humification throughout the year, further indicating that the contribution of terrestrial sources had weakened, while the lake's

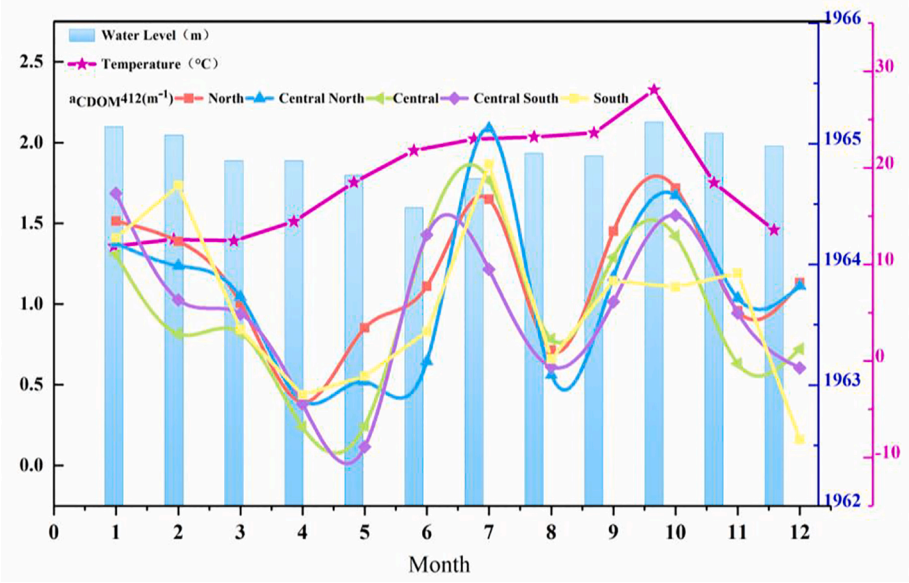

Fig. 6. Monthly $a_{CDOM}(412)$ variation in the five lake regions derived from MODIS/Aqua data and monthly mean water temperature and water level in 2019.

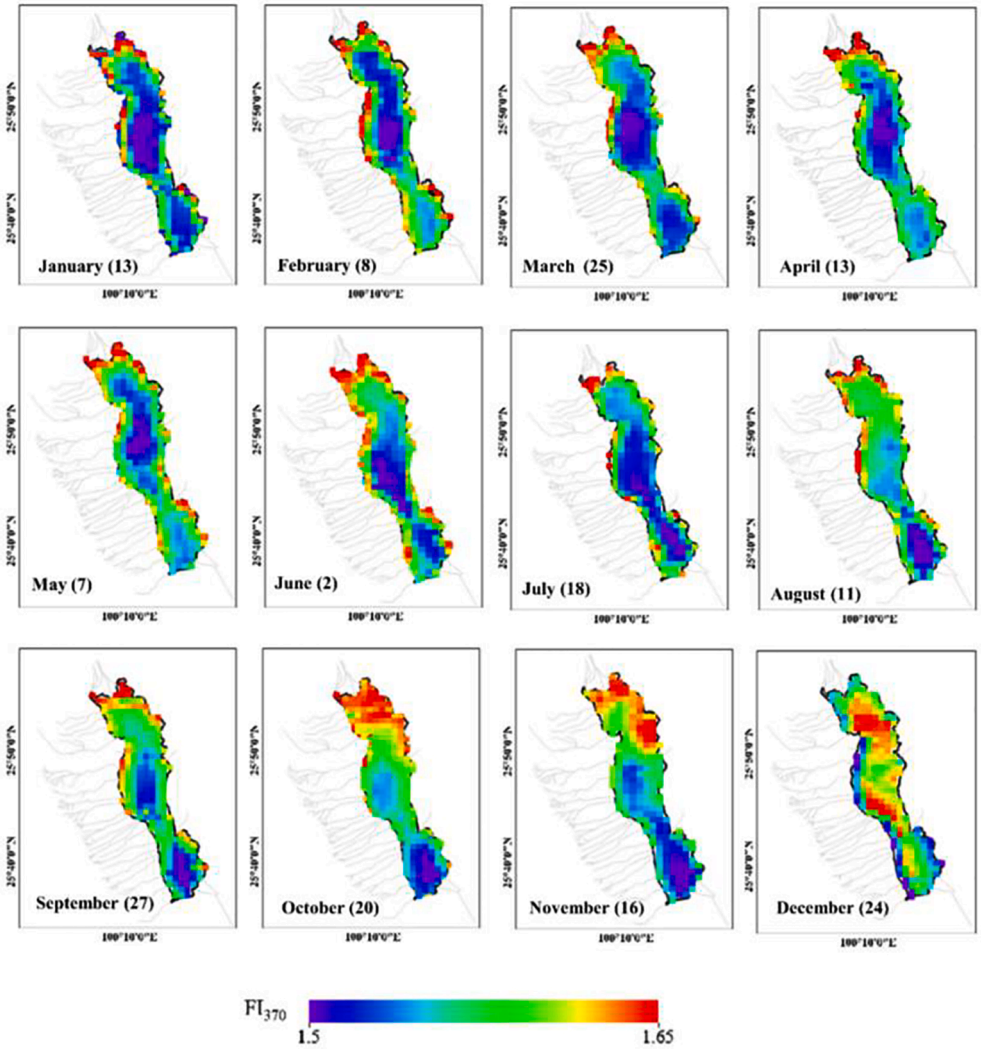

Fig. 7. Monthly distribution of FI_{370} in 2019 derived from the MODIS data.

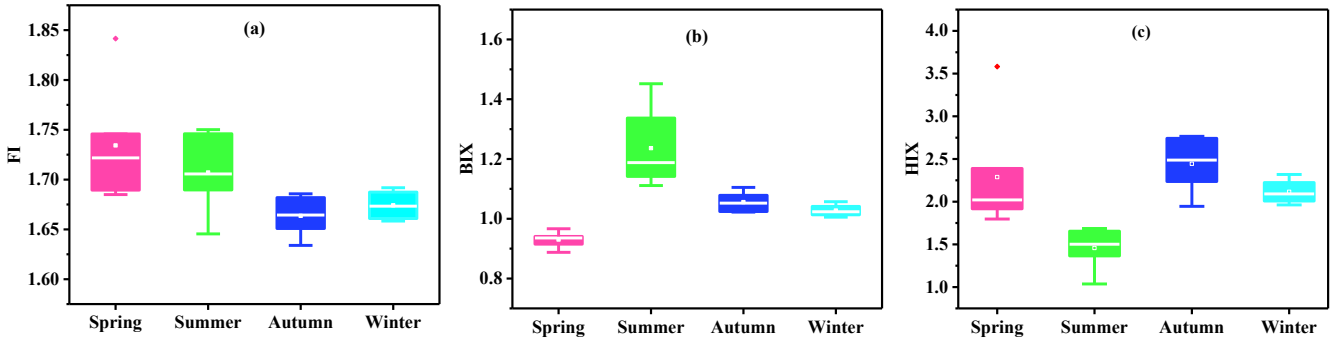

Fig. 8. Box plots of the fluorescence indices (a) FI ,(b) BIX and (c) HIX of Erhai Lake in different seasons.

endogenous metabolic activities had increased.

4. Discussion

4.1. Spatial and temporal patterns of the concentration and sources of CDOM and the environmental significance of CDOM

In this study, higher CDOM concentrations and lower FI_{370} values were found in the northern and western coastal waters than in other parts of Erhai Lake (Figs. 4 and 7). Because there are many villages on the west side of Erhai Lake and different types of regional pollution sources, the river and lake systems are complex. A large quantity of domestic and livestock pollutants is discharged into the area, resulting in an increase in the concentration of organic matter (Guo et al., 2001; Li et al., 2020). In addition, degraded products of aquatic plants are the main source of CDOM in the northern and western parts of the lake. The biomass of algae in the northern areas of the lake is relatively high. FI_{370} is characterised by a biological origin in autumn and winter, which is

mainly affected by the internal release of microorganisms and algae (Tan et al., 2017; Zhang et al., 2009). The higher CDOM concentration in Erhai Lake during summer and autumn than during spring is due to the increase in phytoplankton in the lake (Xu et al., 2020b). Additionally, rainfall caused a large amount of organic matter to be transported into the lake through runoff and rivers. Statistically significant positive correlations were found between precipitation and $a_{CDOM}(412)$ for the entire lake (R^2=0.41, $p<0.05$), indicating that the monthly variation of $a_{CDOM}(412)$ may be affected by monthly precipitation. A similar situation was also found in the Great Lakes region of North America (Xenopoulos et al., 2003). Terrestrial dissolved organic matter originates from the decomposition of soil surface plants and is imported into rivers and lakes through surface runoff and shallow groundwater during rainfall; therefore, the concentration of CDOM decreases significantly during nonrainy seasons. The CDOM of eutrophic lakes is mainly composed of soluble microbial metabolites and humic acid-like DOM. As the degree of eutrophication increases, algae residues and microbial metabolites have more difficulty degrading, and the proportion of humic acid-like DOM increases (Liu et al., 2020; Lyu et al., 2020). Huang et al. found that phytoplankton biomass drives CDOM more strongly than other factors in the eutrophic Lake Taihu (Huang et al., 2019). Therefore, phytoplankton growth and decomposition are important sources of CDOM (Yao et al., 2016; Zhang et al., 2009). On the other hand, the input of external organic matter, nitrogen and phosphorus and the release of sediments provide enough nutrients to support phytoplankton growth; therefore, DOM degradation is offset by uptake (Seitzinger et al., 2005). The rivers that flow into Erhai Lake drain various types of land, including wetlands and land used for agriculture (Zhang and Zhi, 2020). These rivers have high CDOM that likely originates from terrestrial sources (Ma and Li, 2020). In contrast to the western and northern parts of the lake, there are fewer rivers that drain into the eastern part of Erhai Lake, and CDOM and nutrient concentrations are therefore lower. FI_{370} was highest in summer and showed relatively low values in autumn and early winter. In spring and summer, there were some areas with high FI_{370} in the lake, which may be caused by the increase in phytoplankton and microorganisms in the water (Zhang et al., 2020).

Erhai Lake is in a critical period of transition from medium nutrient content to higher eutrophication status (Lin et al., 2021); the nitrogen and phosphorus contents have become key factors affecting the water quality of Erhai Lake; and CDOM is an important source of organic nutrients such as nitrogen and phosphorus in the lake ecosystem (Wen et al., 2016). With the improvement in the treatment of the Erhai Lake Basin, the input of external pollutants has gradually been controlled. However, due to the growth and reproduction of algae and microbial metabolism, CDOM continues to accumulate, always at a high concentration. Therefore, monitoring changes in the concentrations and sources of CDOM in water bodies is the basis for understanding the nutrient cycle in lake ecosystems (Hanson et al., 2007). Overall, the development from laboratory analysis to remote sensing data combined with water quality inversion models has clear potential for understanding the nutrient cycle on larger scales. It can not only help the local government manage water quality but also provide support for research on global climate change and the impact of human activities, which is of great value.

4.2. Rationality and applicability of the CDOM retrieval model

The CDOM model proposed in this study was based on MODIS/Aqua data and field-measured CDOM concentration and fluorescence data. By comparing possible bands and band combinations, an empirical algorithm for $a_{CDOM}(412)$ and an empirical and semi-empirical algorithm for FI_{370} were developed. For the $a_{CDOM}(412)$ models, ((Rrs(645) + Rrs (469)/Rrs(555)) performed better than the other band combinations (Table 2 and Figure S1). According to previous studies, for lakes that were greatly affected by internal source releases and land source input (Stedmon et al., 2006), the performance of the empirical algorithm can be significantly improved by selecting at least one wavelength band longer than 600 nm (Aurin and Dierssen, 2012; Del Castillo and Miller, 2008; Zhu et al., 2014) because the red or near-infrared band can help to better analyse detrital particles. The blue and green bands have been determined to be sensitive to CDOM (Chen et al., 2017b; Sun et al., 2011), which confirmed the rationality of the CDOM concentration inversion model of Erhai Lake.

When developing the FI_{370} model, the influence of the Chl-a concentration on FI_{370} was considered to be important. The absorption of CDOM can extend to the blue band of visible light, which overlaps with the absorption of phytoplankton Chl-a. Therefore, this study divided the measured data into two data sets. One data set (Chl-a>10 μg/L) contained 30 data points, and the other data set (Chl-a<10 μg/L) contained 29 data points. Based on the different Chl-a concentrations of the two data sets, the CDOM absorption coefficient $a_{CDOM}(412)$ was used to develop the models (Tables 4 and 5).

Combined with previous studies on the characteristic bands of CDOM inversion, the accuracy of the model has been improved. For Chl-a<10 μg/L, the model Rrs(555)/Rrs(469) of $a_{CDOM}(412)$ had the best effect (R^2=0.76). The accuracy of the model is close to that of Model 1. The reflectivity of 469 nm and 555 nm was also used. Similar band combinations have been used in the research of other bays or cleaner water bodies. Tehrani et al. evaluated empirical algorithms and found that compared with that of the Rrs(490)/Rrs(555) band ratio algorithm, the performance of using Rrs(510)/Rrs(555) was better in the northern Gulf of Mexico (Tehrani et al., 2013). For Chl-a>10 μg/L, the empirical band ratio of Rrs(531)/Rrs(555) (R^2=0.313) had a higher accuracy and significantly better performance than the blue-green band ratio (R^2=0.167). A previous study used a similar band ratio Rrs(531)/Rrs (551) to retrieve the CDOM concentration in the Bohai Sea, China (Yu et al., 2017). In the results of the CDOM retrieval model for Chl-a classification, the accuracy was higher for Chl-a<10 μg/L than for Chl-a>10 μg/L, indicating that a higher concentration of Chl-a in the water body affects the model. A similar result was found, i.e., in a relatively clean water body, CDOM retrieval was better than in a turbid water body, which was due to the influence of suspended solids (Xu et al., 2018). However, for the data set under different Chl-a concentrations, (Rrs (645)+Rrs(469))/Rrs(555) from Model 1 showed relatively good estimation results. Fluorescence spectra showed significant differences in different types of water bodies, providing the possibility to track the evolution of CDOM. FI_{370} can reflect the sources of CDOM from a qualitative and semiquantitative perspective. For the development of the FI_{370} algorithm, Rrs(469) and Rrs(555) were the important variables reflecting FI_{370}. At 555 nm, the change in reflectivity was mainly due to the presence of phytoplankton or debris driving the light scattering of particles (Mannino et al., 2014). Compared with that at other bands, the reflectance at 645 nm was most affected by CDOM absorption, closely related to the influence of phytoplankton. The band ratio algorithm including 645 nm exhibited a good estimation effect in this area. In addition, Rrs(859) and Rrs(555) in the algorithm had a strong correlation with the concentration of Chl-a. The reason is that Chl-a has obvious peaks and troughs in absorbance or reflectance (Ha et al., 2017; Li et al., 2012; Moutier et al., 2019), such as those in the near-infrared and green bands, which were used when establishing lake water quality retrieval models (Chen et al., 2011b; Ha et al., 2017; Hu et al., 2012). While developing the FI_{370} algorithm, this study tried to introduce the APPEL model as a variable to the algorithm to improve the inversion accuracy. The semi-empirical model has advantages when there is a large number of phytoplankton in eutrophic water. Fluorescent substances are one of the important products of phytoplankton degradation, and the number of phytoplankton is often reflected by the concentration of Chl-a. Therefore, after the APPEL model was used as a variable, the algorithm became a semi-empirical algorithm, similar to the algorithm derived from coupling, and the estimation accuracy was optimised compared with that of the empirical algorithm. In addition, the semi-empirical algorithm was based on theoretical knowledge and water

Table 4
Regression results show that the $a_{CDOM}(412)$ can be predicted by models with various bands and band ratios when Chl-a>10 μg/L.

Independent Variables	R^2	Equation Coefficients Y = b0 + b1(x1) + b2(x2) b0	b1	b2	b3	Outlier	RMSE	Adj.R^2
Chl-a>10 μg/L $\ln(a_{CDOM}(412))$ models								
B10/B4	0.23	3.67	−4.54				0.66	0.17
B11/B4	0.31	15.35	−16.33				0.62	0.27
B8/B12	0.17	1.46	−1.64				0.76	0.09
B4/B3	0.17	−2.69	2.16				0.69	0.11
(B3+B1)/B4	0.39	4.83	−2.85				0.59	0.35
(B10-B4)/(B10+B4)	0.24	−0.86	8.00				0.66	0.19

Table 5
Regression results show that $a_{CDOM}(412)$ can be predicted by models with various bands and band ratios when Chl-a<10 μg/L.

Independent		Equation Coefficients Y = b0 + b1(x1) + b2(x2)					
		b0	b1	b2	Outlier	RMSE	Adj. R^2
Chl-a<10 μg/L $\ln(a_{CDOM}(412))$ models							
B10/B4	0.70	5.02	−6.04			0.57	0.69
B8/B12	0.68	2.56	−2.83			0.59	0.66
B8/B10	0.62	5.16	−4.56			0.64	0.61
B8/B4	0.63	2.29	−2.39			0.64	0.61
B4/B3	0.76	−5.15	4.25			0.51	0.75
(B3+B1)/B4	0.74	7.61	−4.47			0.53	0.73
(B10-B4)/(B10+B4)	0.74	−1.08	11.22			0.53	0.72

colour spectrum information, which had certain physical significance. The bio-optical characteristics of water bodies were different in different regions, and the factors affecting the temporal and spatial distribution of CDOM in lake ecosystems were complex and closely related to lake biogeochemical processes (Matsuoka et al., 2012), such as hydraulic conditions, lake mixing and stratification, sediment suspension, phytoplankton growth and river input (Alcântara et al., 2017; Brezonik et al., 2015; Lapierre and Frenette, 2009; Liu et al., 2015b). The applicability of the retrieval model may change (Chen et al., 2019a). Future research still needs to develop a more in-depth understanding of the mechanisms of spatial and temporal changes in CDOM concentrations and sources in Erhai Lake. Using the CDOM models proposed here, we can observe changes in water quality, which can provide data and scientific support for local environmental departments to make more reasonable and effective decisions.

5. Conclusions

In this study, based on MODIS/Aqua data combined with field data, inversion models of the CDOM concentration and FI_{370} in Erhai Lake were developed, the temporal and spatial distributions of the lake's CDOM concentrations and sources were analysed, and the rationality and applicability of the models were discussed. The main conclusions are as follows:

(1) Based on (Rrs(645)+Rrs(469))/Rrs(555), an inversion model of CDOM concentration was developed (R^2=0.507, RMSE=0.2 m^{-1}). After verification, it was found that the $a_{CDOM}(412)$ model performs well. For the FI_{370} model, the empirical algorithm (Rrs(469)-Rrs(555))/(Rrs(469)+Rrs(555)) has an R^2=0.505 and an RMSE=0.030. On the basis of the band ratio of Rrs(645)/Rrs (469), the APPEL model of Chl-a was introduced, and a semi-empirical model of FI_{370} was developed, which obtained high model accuracy (R^2=0.550, RMSE=0.037).

(2) Based on model inversion, the CDOM concentration and the FI_{370} information of Erhai Lake in 2013–2019 were obtained. The concentration of CDOM in Erhai Lake was higher in the northern lake area and the western coast and lower in the eastern and southern regions. The concentration of CDOM in the northern and western coastal waters during summer was significantly higher than that during other seasons. FI_{370} shows that the western part of Erhai Lake was more terrestrial-sourced than the eastern part, and the northern and western lake areas had higher fluorescence indices because CDOM was affected by the combined effects of the soluble microbial metabolites in the aquatic plant distribution area and the internal release from rivers and sediments into the lake in the western area.

(3) For the application of the CDOM concentration model, it was confirmed that the model performs well at different concentration levels. The band ratios Rrs(645))/Rrs(555) and (Rrs(645)+Rrs(469))/Rrs(555) performed best under Chl-a<10 μg/L and Chl-a>10 μg/L, respectively. In addition, the research results found that the performance of the model was significantly improved for Chl-a<10 μg/L (R^2=0.76). Although the accuracy of the model was reduced for Chl-a>10 μg/L, the model is still applicable.

This study provides a feasible remote sensing method that developed algorithms for studying the temporal and spatial dynamics of the CDOM concentration and fluorescence indices in Erhai Lake, which is helpful to obtain the CDOM concentration and sources information. The research results can provide a theoretical basis for the protection and management of Erhai Lake and a practical reference.

Funding

This research was jointly supported by the National Natural Science Foundation of China (No. U1902207), the Yunnan Key Laboratory of Pollution Process and Management of Plateau Lake-Watershed (2020-02-2-W2, 2020-02-2-W3), the National Major Science and Technology Program for Water Pollution Control and Treatment (2018ZX07701001-17), and the China Postdoctoral Science Foundation (2019M660521).

CRediT authorship contribution statement

Hao Zhang: Writing - original draft, Methodology, Writing - review & editing. **Bo Yao:** Methodology, Software, Conceptualization. **Shengrui Wang:** Writing - review & editing, Supervision. **Guoqiang Wang:** Writing - original draft.

Declaration of Competing Interest

The authors declare that they have no known competing financial interests or personal relationships that could have appeared to influence the work reported in this paper.

Acknowledgements

This research was jointly supported by the National Natural Science Foundation of China (No. U1902207) and Yunnan Key Laboratory of Pollution Process and Management of Plateau Lake-Watershed (2020-02-2-W2, 2020-124A-W2).

Appendix A. Supplementary data

Supplementary data to this article can be found online at https://doi.org/10.1016/j.ecolind.2021.108180.

References

Alcântara, E., Bernardo, N., Rodrigues, T., Watanabe, F., 2017. Modeling the spatio-temporal dissolved organic carbon concentration in Barra Bonita reservoir using OLI/Landsat-8 images. Model. Earth Syst. Environ. 3 (1) https://doi.org/10.1007/s40808-017-0275-2.

Aurin, D.A., Dierssen, H.M., 2012. Advantages and limitations of ocean color remote sensing in CDOM-dominated, mineral-rich coastal and estuarine waters. Remote Sens. Environ. 125, 181–197.

Baines, S.B., Pace, M.L., 1991. The production of dissolved organic matter by phytoplankton and its importance to bacteria: patterns across marine and freshwater systems. Limnol. Oceanogr. 36 (6), 1078–1090.

Brezonik, P., Menken, K.D., Bauer, M., 2005. Landsat-based remote sensing of lake water quality characteristics, including chlorophyll and colored dissolved organic matter (CDOM). Lake Reservoir Manage. 21 (4), 373–382.

Brezonik, P.L., Olmanson, L.G., Finlay, J.C., Bauer, M.E., 2015. Factors affecting the measurement of CDOM by remote sensing of optically complex inland waters. Remote Sens. Environ. 157, 199–215.

Chen, H., Zheng, B., Song, Y., Qin, Y., 2011a. Correlation between molecular absorption spectral slope ratios and fluorescence humification indices in characterizing CDOM. Aquat. Sci. 73 (1), 103–112.

Chen, J., Zhu, W.-N., Tian, Y.Q., Yu, Q., 2017a. Estimation of colored dissolved organic matter from landsat-8 imagery for complex inland water: case study of Lake Huron. IEEE Trans. Geosci. Remote Sens. 55 (4), 2201–2212.

Chen, J., Zhu, W., Tian, Y.Q., Yu, Q., Zheng, Y., Huang, L., 2017b. Remote estimation of colored dissolved organic matter and chlorophyll-a in Lake Huron using Sentinel-2 measurements. J. Appl. Remote Sens. 11 (03), 1. https://doi.org/10.1117/1.JRS.11.036007.

Chen, J., et al., 2019. Applicability evaluation of Landsat-8 for estimating low concentration colored dissolved organic matter in inland water. Geocarto international., 1-15.

J. Chen W. Zhu Y. Zheng Y.Q. Tian Q. Yu Monitoring seasonal variations of colored dissolved organic matter for the Saginaw River based on Landsat-8 data 19 1 2019 274 281.

Chen, S., Fang, L., Li, H., Chen, W., Huang, W., 2011b. Evaluation of a three-band model for estimating chlorophyll-a concentration in tidal reaches of the Pearl River Estuary, China. ISPRS J. Photogrammetry Remote Sens. 66 (3), 356–364.

Cherukuru, N., Ford, P.W., Matear, R.J., Oubelkheir, K., Clementson, L.A., Suber, K., Steven, A.D.L., 2016. Estimating dissolved organic carbon concentration in turbid coastal waters using optical remote sensing observations. Int. J. Appl. Earth Observation Geoinformation 52, 149–154.

Chiu, T.P., et al., 2019. Fluorescence Characteristics of Dissolved Organic Matter (DOM) in Percolation Water and Lateral Seepage Affected by Soil Solution (S-S) in a Lysimeter Test. Sensors (Basel). 19.

Claustre, H., Fell, F., Oubelkheir, K., Prieur, L., Sciandra, A., Gentili, B., Babin, M., 2000. Continuous monitoring of surface optical properties across a geostrophic front: biogeochemical inferences. Limnol. Oceanogr. 45 (2), 309–321.

Conmy, R.N., Coble, P.G., Chen, R.F., Gardner, G.B., 2004. Optical properties of colored dissolved organic matter in the Northern Gulf of Mexico. Mar. Chem. 89 (1-4), 127–144.

D'Sa, E.J., Overton, E.B., Lohrenz, S.E., Maiti, K., Turner, R.E., Freeman, A., 2016. Changing dynamics of dissolved organic matter fluorescence in the northern gulf of mexico following the deepwater horizon oil spill. Environ. Sci. Technol. 50 (10), 4940–4950.

Del Castillo, C.E., Miller, R.L., 2008. On the use of ocean color remote sensing to measure the transport of dissolved organic carbon by the Mississippi River Plume. Remote Sens. Environ. 112 (3), 836–844.

Dörnhöfer, K., Oppelt, N., 2016. Remote sensing for lake research and monitoring – Recent advances. Ecol. Indicat. 64, 105–122.

Downing, B.D., Boss, E., Bergamaschi, B.A., Fleck, J.A., Lionberger, M.A., Ganju, N.K., Schoellhamer, D.H., Fujii, R., 2009. Quantifying fluxes and characterizing compositional changes of dissolved organic matter in aquatic systems in situ using combined acoustic and optical measurements. Limnol. Oceanogr. 7 (1), 119–131.

El-Alem, A., Chokmani, K., Laurion, I., El-Adlouni, S.E., 2012. Comparative analysis of four models to estimate chlorophyll-a concentration in case-2 waters using moderate resolution imaging spectroradiometer (MODIS) imagery. Remote Sens. 4 (8), 2373–2400.

Fellman, J.B., Hood, E., Spencer, R.G.M., 2010. Fluorescence spectroscopy opens new windows into dissolved organic matter dynamics in freshwater ecosystems: a review. Limnol. Oceanogr. 55 (6), 2452–2462.

Gholizadeh, M., Melesse, A., Reddi, L., 2016. A comprehensive review on water quality parameters estimation using remote sensing techniques. Sensors 16 (8), 1298. https://doi.org/10.3390/s16081298.

Gitelson, A.A., Dall'Olmo, G., Moses, W., Rundquist, D.C., Barrow, T., Fisher, T.R., Gurlin, D., Holz, J., 2008. A simple semi-analytical model for remote estimation of chlorophyll-a in turbid waters: validation. Remote Sens. Environ. 112 (9), 3582–3593.

Griffin, C.G., McClelland, J.W., Frey, K.E., Fiske, G., Holmes, R.M., 2018. Quantifying CDOM and DOC in major Arctic rivers during ice-free conditions using Landsat TM and ETM+ data. Remote Sens. Environ. 209, 395–409.

Guo, H.C., Liu, L., Huang, G.H., Fuller, G.A., Zou, R., Yin, Y.Y., 2001. A system dynamics approach for regional environmental planning and management: a study for the Lake Erhai Basin. J. Environ. Manage. 61 (1), 93–111.

Ha, N.T.T., Thao, N.T.P., Koike, K., Nhuan, M.T., 2017. Selecting the Best Band Ratio to Estimate Chlorophyll-a Concentration in a Tropical Freshwater Lake Using Sentinel 2A Images from a Case Study of Lake Ba Be (Northern Vietnam). ISPRS Int. J. Geo-Information. 6 (9), 290. https://doi.org/10.3390/ijgi6090290.

Han, X., Feng, L., Chen, X., Yesou, H., 2014. MERIS observations of chlorophyll-a dynamics in Erhai Lake between 2003 and 2009. Int. J. Remote Sens. 35 (24), 8309–8322.

Hanson, C.E., Waite, A.M., Thompson, P.A., Pattiaratchi, C.B., 2007. Phytoplankton community structure and nitrogen nutrition in Leeuwin Current and coastal waters off the Gascoyne region of Western Australia. Deep Sea Res. Part II: Top. Stud. Oceanogr. 54 (8-10), 902–924.

Hou, X., Feng, L., Duan, H., Chen, X., Sun, D., Shi, K., 2017. Fifteen-year monitoring of the turbidity dynamics in large lakes and reservoirs in the middle and lower basin of the Yangtze River, China. Remote Sens. Environ. 190, 107–121.

Hu, C., Lee, Z., Franz, B., 2012. Chlorophylla algorithms for oligotrophic oceans: A novel approach based on three-band reflectance difference. J. Geophys. Res. Oceans 117 (C1). https://doi.org/10.1029/2011JC007395.

Huang, C., Zhang, Y., Huang, T., Yang, H., Li, Y., Zhang, Z., He, M., Hu, Z., Song, T., Zhu, A.-X., 2019. Long-term variation of phytoplankton biomass and physiology in Taihu lake as observed via MODIS satellite. Water Res. 153, 187–199.

Huguet, A., Vacher, L., Relexans, S., Saubusse, S., Froidefond, J.M., Parlanti, E., 2009. Properties of fluorescent dissolved organic matter in the Gironde Estuary. Org. Geochem. 40 (6), 706–719.

Ji, N., Wang, S., Zhang, L., 2017. Characteristics of dissolved organic phosphorus inputs to freshwater lakes: a case study of Lake Erhai, southwest China. Sci. Total Environ. 601-602, 1544–1555.

Jing, Y., Zhang, Y., Hu, M., Chu, Q., Ma, R., 2019. MODIS-satellite-based analysis of long-term temporal-spatial dynamics and drivers of algal blooms in a plateau lake Dianchi, China. Remote Sens. 11 (21), 2582. https://doi.org/10.3390/rs11212582.

Klein, I., Gessner, U., Dietz, A.J., Kuenzer, C., 2017. Global WaterPack – A 250 m resolution dataset revealing the daily dynamics of global inland water bodies. Remote Sens. Environ. 198, 345–362.

Kowalczuk, P., Stoń-Egiert, J., Cooper, W.J., Whitehead, R.F., Durako, M.J., 2005. Characterization of chromophoric dissolved organic matter (CDOM) in the Baltic Sea by excitation emission matrix fluorescence spectroscopy. Mar. Chem. 96 (3-4), 273–292.

Lapierre, J.-F., Frenette, J.-J., 2009. Effects of macrophytes and terrestrial inputs on fluorescent dissolved organic matter in a large river system. Aquat. Sci. 71 (1), 15–24.

Lei, X., Pan, J., Devlin, A., 2019. Characteristics of absorption spectra of chromophoric dissolved organic matter in the pearl river estuary in spring. Remote Sens. 11 (13), 1533. https://doi.org/10.3390/rs11131533.

Li, J., Bai, Y., Alatalo, J.M., 2020. Impacts of rural tourism-driven land use change on ecosystems services provision in Erhai Lake Basin, China. Ecosyst. Services. 42, 101081. https://doi.org/10.1016/j.ecoser.2020.101081.

Li, Y., Wang, Q., Wu, C., Zhao, S., Xu, X., Wang, Y., Huang, C., 2012. Estimation of chlorophyll a concentration using NIR/Red Bands of MERIS and classification procedure in inland turbid water. IEEE Trans. Geosci. Remote Sens. 50 (3), 988–997.

Lin, S.-S., Shen, S.-L., Zhou, A., Lyu, H.-M., 2020. Sustainable development and environmental restoration in Lake Erhai, China. J. Clean. Prod. 258, 120758. https://doi.org/10.1016/j.jclepro.2020.120758.

Lin, S.-S., Shen, S.-L., Zhou, A., Lyu, H.-M., 2021. Assessment and management of lake eutrophication: a case study in Lake Erhai, China. Sci. Total Environ. 751, 141618. https://doi.org/10.1016/j.scitotenv.2020.141618.

Liu, W., Wang, S., Zhang, L., Ni, Z., Zhao, H., Jiao, L.X., 2015a. Phosphorus release characteristics of sediments in Erhai Lake and their impact on water quality. Environ. Earth Sci. 74 (5), 3753–3766.

Liu, D., Pan, D., Bai, Y., He, X., Wang, D., Zhang, L., 2015b. Variation of dissolved organic carbon transported by two Chinese rivers: the Changjiang river and yellow river. Mar. Pollut. Bull. 100 (1), 60–69.

Liu, D., Du, Y., Yu, S., Luo, J., Duan, H., 2020. Human activities determine quantity and composition of dissolved organic matter in lakes along the Yangtze River. Water Res. 168, 115132. https://doi.org/10.1016/j.watres.2019.115132.

Liu, X., Zhang, Y., Yin, Y., Wang, M., Qin, B., 2013. Wind and submerged aquatic vegetation influence bio-optical properties in large shallow Lake Taihu, China. J. Geophys. Res. Biogeosci. 118 (2), 713–727.

Lyu, L., Wen, Z., Jacinthe, P.-A., Shang, Y., Zhang, N., Liu, G., Fang, C., Hou, J., Song, K., 2020. Absorption characteristics of CDOM in treated and non-treated urban lakes in Changchun, China. Environ. Res. 182, 109084. https://doi.org/10.1016/j.envres.2019.109084.

Ma, Y., Li, S., 2020. Spatial and temporal comparisons of dissolved organic matter in river systems of the Three Gorges Reservoir region using fluorescence and

UV–Visible spectroscopy. Environ. Res. 189, 109925. https://doi.org/10.1016/j.envres.2020.109925.
Mannino, A., Novak, M.G., Hooker, S.B., Hyde, K., Aurin, D., 2014. Algorithm development and validation of CDOM properties for estuarine and continental shelf waters along the northeastern U.S. coast. Remote Sens. Environ. 152, 576–602.
Matsuoka, A., Bricaud, A., Benner, R., Para, J., Sempéré, R., Prieur, L., Bélanger, S., Babin, M., 2012. Tracing the transport of colored dissolved organic matter in water masses of the Southern Beaufort Sea: relationship with hydrographic characteristics. Biogeosciences. 9 (3), 925–940.
McKnight, D.M., Boyer, E.W., Westerhoff, P.K., Doran, P.T., Kulbe, T., Andersen, D.T., 2001. Spectrofluorometric characterization of dissolved organic matter for indication of precursor organic material and aromaticity. Limnol. Oceanogr. 46 (1), 38–48.
Miao, S., Lyu, H., Wang, Q., Li, Y., Wu, Z., Du, C., Xu, J., Bi, S., Mu, M., Lei, S., 2019. Estimation of terrestrial humic-like substances in inland lakes based on the optical and fluorescence characteristics of chromophoric dissolved organic matter (CDOM) using OLCI images. Ecol. Indicat. 101, 399–409.
Moutier, W., Thomalla, S., Bernard, S., Wind, G., Ryan-Keogh, T., Smith, M., 2019. Evaluation of Chlorophyll-a and POC MODIS aqua products in the Southern Ocean. Remote Sens. 11 (15), 1793. https://doi.org/10.3390/rs11151793.
O'Reilly, J.E., Werdell, P.J., 2019. Chlorophyll algorithms for ocean color sensors - OC4, OC5 & OC6. Remote Sens. Environ. 229, 32–47.
Ruddick, K.G., et al., 2004. Atmospheric correction of SeaWiFS imagery for turbid coastal and inland waters. Acta Oceanol. Sin. 23, 609–615.
Seitzinger, S.P., Harrison, J.A., Dumont, E., Beusen, A.H.W., Bouwman, A.F., 2005. Sources and delivery of carbon, nitrogen, and phosphorus to the coastal zone: an overview of Global Nutrient Export from Watersheds (NEWS) models and their application. Glob. Biogeochem. Cycles 19 (4).
Stedmon, C.A., Markager, S., Søndergaard, M., Vang, T., Laubel, A., Borch, N.H., Windelin, A., 2006. Dissolved Organic Matter (DOM) export to a temperate estuary: seasonal variations and implications of land use. Estuaries Coasts 29 (3), 388–400.
Sun, D.Y., Li, Y.M., Wang, Q., Lu, H., Le, C.F., Huang, C.C., Gong, S.Q., 2011. A neural-network model to retrieve CDOM absorption from in situ measured hyperspectral data in an optically complex lake: Lake Taihu case study. Int. J. Remote Sens. 32 (14), 4005–4022.
Tan, W., Liu, P., Liu, Y., Yang, S., Feng, S., 2017. A 30-year assessment of phytoplankton blooms in Erhai Lake using Landsat imagery: 1987 to 2016. Remote Sens. 9 (12), 1265. https://doi.org/10.3390/rs9121265.
Tehrani, N., D'Sa, E., Osburn, C., Bianchi, T., Schaeffer, B., 2013. Chromophoric dissolved organic matter and dissolved organic carbon from sea-viewing wide field-of-view sensor (SeaWiFS), moderate resolution imaging spectroradiometer (MODIS) and MERIS sensors: case study for the Northern Gulf of Mexico. Remote Sens. 5 (3), 1439–1464.
Wang, S., Zhang, L., Ni, L., Zhao, H., Jiao, L., Yang, S., Guo, L., Shen, J., 2015a. Ecological degeneration of the Erhai Lake and prevention measures. Environ. Earth Sci. 74 (5), 3839–3847.
Wang, S., et al., 2015b. Suitability of the retrieval models for estimating chlorophyll concentration in Lake Taihu. J. Lake Sci. 27, 150–162.
Wang, S., Li, J., Zhang, B., Spyrakos, E., Tyler, A.N., Shen, Q., Zhang, F., Kuster, T., Lehmann, M.K., Wu, Y., Peng, D., 2018. Trophic state assessment of global inland waters using a MODIS-derived Forel-Ule index. Remote Sens. Environ. 217, 444–460.
Wang, X., Yang, W., 2019. Water quality monitoring and evaluation using remote-sensing techniques in China: A systematic review. Ecosyst. Health Sustain. 5 (1), 47–56.
Wang, H., Wen, Z., Zhang, Z., Zhang, X., Fu, H., Cao, Y.u., Ni, L., Cao, T.e., Li, K., 2020. Environmental vs. spatial drivers of submerged macrophyte community assembly in different seasons and water depths in a mesotrophic bay of Erhai Lake, China. Ecol. Indicat. 117, 106696. https://doi.org/10.1016/j.ecolind.2020.106696.
Wen, Z.D., Song, K.S., Zhao, Y., Du, J., Ma, J.H., 2016. Influence of environmental factors on spectral characteristics of chromophoric dissolved organic matter (CDOM) in Inner Mongolia Plateau, China. Hydrol. Earth Syst. Sci. 20 (2), 787–801.
Wu, G., Cui, L., He, J., Duan, H., Fei, T., Liu, Y., 2013. Comparison of MODIS-based models for retrieving suspended particulate matter concentrations in Poyang Lake, China. Int. J. Appl. Earth Observation Geoinformation. 24, 63–72.
Xenopoulos, M.A., Lodge, D.M., Frentress, J., Kreps, T.A., Bridgham, S.D., Grossman, E., Jackson, C.J., 2003. Regional comparisons of watershed determinants of dissolved organic carbon in temperate lakes from the Upper Great Lakes region and selected regions globally. Limnol. Oceanogr. 48 (6), 2321–2334.
Xu, J., Fang, C., Gao, D., Zhang, H., Gao, C., Xu, Z., Wang, Y., 2018. Optical models for remote sensing of chromophoric dissolved organic matter (CDOM) absorption in Poyang Lake. ISPRS J. Photogrammetry Remote Sens. 142, 124–136.
Xu, J., Gao, C., Wang, Y., 2020a. Extraction of spatial and temporal patterns of concentrations of chlorophyll-a and total suspended matter in Poyang lake using GF-1 Satellite data. Remote Sens. 12 (4), 622. https://doi.org/10.3390/rs12040622.
Xu, X., Zhang, Y., Chen, Q., Li, N., Shi, K., Zhang, Y., 2020b. Regime shifts in shallow lakes observed by remote sensing and the implications for management. Ecol. Indicat. 113, 106285. https://doi.org/10.1016/j.ecolind.2020.106285.
Xue, K., Ma, R., Duan, H., Shen, M., Boss, E., Cao, Z., 2019. Inversion of inherent optical properties in optically complex waters using sentinel-3A/OLCI images: a case study using China's three largest freshwater lakes. Remote Sens. Environ. 225, 328–346.
Yang, S., Chen, X., Lu, J., Hou, X., Li, W., Xu, Q., 2021. Impacts of agricultural topdressing practices on cyanobacterial bloom phenology in an early eutrophic plateau Lake, China. J. Hydrol. 594, 125952. https://doi.org/10.1016/j.jhydrol.2020.125952.
Yao, B., Hu, C., Liu, Q., 2016. Fluorescent components and spatial patterns of chromophoric dissolved organic matters in Lake Taihu, a large shallow eutrophic lake in China. Environ. Sci. Pollut. Res. 23 (22), 23057–23070.
Yu, X., Xiao, B., Liu, X., Wang, Y., Cui, B., Liu, X., 2017. Retrieval of remotely sensed sea surface salinity using MODIS data in the Chinese Bohai Sea. Int. J. Remote Sens. 38 (23), 7357–7373.
Zepp, R.G., Sheldon, W.M., Moran, M.A., 2004. Dissolved organic fluorophores in southeastern US coastal waters: correction method for eliminating Rayleigh and Raman scattering peaks in excitation–emission matrices. Mar. Chem. 89 (1-4), 15–36.
Zhang, J., Zhi, M., 2020. Effects of basin nutrient discharge variations coupled with climate change on water quality in Lake Erhai, China. Environ. Sci. Pollut. Res. 27 (35), 43700–43710.
Zhang, L., Xu, K., Wang, S., Wang, S., Li, Y., Li, Q., Meng, Z., 2018a. Characteristics of dissolved organic nitrogen in overlying water of typical lakes of Yunnan Plateau, China. Ecol. Indicat. 84, 727–737.
Zhang, Y., van Dijk, M.A., Liu, M., Zhu, G., Qin, B., 2009. The contribution of phytoplankton degradation to chromophoric dissolved organic matter (CDOM) in eutrophic shallow lakes: field and experimental evidence. Water Res. 43 (18), 4685–4697.
Zhang, Y., Zhang, E., Yin, Y., van Dijk, M.A., Feng, L., Shi, Z., Liu, M., Qina, B., 2010. Characteristics and sources of chromophoric dissolved organic matter in lakes of the Yungui Plateau, China, differing in trophic state and altitude. Limnol. Oceanogr. 55 (6), 2645–2659.
Zhang, Y., Zhou, Y., Shi, K., Qin, B., Yao, X., Zhang, Y., 2018b. Optical properties and composition changes in chromophoric dissolved organic matter along trophic gradients: Implications for monitoring and assessing lake eutrophication. Water Res. 131, 255–263.
Zhang, Y., Shi, K., Zhou, Q., Zhou, Y., Zhang, Y., Qin, B., Deng, J., 2020. Decreasing underwater ultraviolet radiation exposure strongly driven by increasing ultraviolet attenuation in lakes in eastern and southwest China. Sci. Total Environ. 720, 137694. https://doi.org/10.1016/j.scitotenv.2020.137694.
Zhu, W., Yu, Q., Tian, Y.Q., Becker, B.L., Zheng, T., Carrick, H.J., 2014. An assessment of remote sensing algorithms for colored dissolved organic matter in complex freshwater environments. Remote Sens. Environ. 140, 766–778.
Zsolnay, A., et al., 1999. Differentiating with fluorescence spectroscopy the sources of dissolved organic matter in soils subjected to drying. 38, 45-50.